Dalton Transactions

PERSPECTIVE

View Article Online
View Journal | View Issue

Cite this: *Dalton Trans.*, 2015, **44**, 16195

An ethane-bridged porphyrin dimer as a model of di-heme proteins: inorganic and bioinorganic perspectives and consequences of heme–heme interactions†

Debangsu Sil and Sankar Prasad Rath*

Received 9th March 2015,
Accepted 2nd June 2015

DOI: 10.1039/c5dt00947b

www.rsc.org/dalton

Interaction between heme centers has been cleverly implemented by Nature in order to regulate different properties of multiheme cytochromes, thereby allowing them to perform a wide variety of functions. Our broad interest lies in unmasking the roles played by heme–heme interactions in modulating different properties *viz.*, metal spin state, redox potential *etc.*, of the individual heme centers using an ethane-bridged porphyrin dimer as a synthetic model of dihemes. The large differences in the structure and properties of the diheme complexes, as compared to the monoheme analogs, provide unequivocal evidence of the role played by heme–heme interactions in the dihemes. This Perspective provides a brief account of our recent efforts to explore these interesting aspects and the subsequent outcomes.

1. Introduction

1.1 Multiheme cytochromes and enzymes

The family of the multiheme cytochrome c represents an extensive class of proteins with vital roles in electron transfer and enzymatic catalysis.[1–3] The majority of the multiheme

Department of Chemistry, Indian Institute of Technology Kanpur, Kanpur 208016, India. E-mail: sprath@iitk.ac.in; Fax: +91-5122596806; Tel: +91-5122597251

†Dedicated to Professor Animesh Chakravorty on the occasion of his 80th birthday.

Debangsu Sil

Debangsu Sil earned his bachelor's degree in chemistry from the University of Burdwan in 2007 and master's degree from the Indian Institute of Technology, Kanpur in 2009. He is currently pursuing his PhD, studying diiron and dimanganese bisporphyrins as models for diheme cytochromes, in Prof. S. P. Rath's laboratory at the Indian Institute of Technology, Kanpur.

Sankar Prasad Rath

Sankar Prasad Rath received his bachelor and master degrees from the Calcutta University in 1992 and 1994, respectively, and obtained his PhD with Prof. A. Chakravorty in 1999 from the Indian Association for the Cultivation of Science (IACS), Kolkata. After a postdoctoral study with Prof. A. L. Balch at the University of California, Davis, he joined the Department of Chemistry at the Indian Institute of Technology Kanpur in December 2004 where he is a full professor since 2014. He is a recipient of P. K. Kelkar Research Fellowship for young faculty (2009–12), Alexander von Humboldt Fellowship for Experienced Researcher (2012) and Chemical Research Society of India (CRSI) Bronze medal (2014). His current research interests are bioinorganic modeling of multi-heme proteins/enzymes, binding and activation of small molecules, electron and energy transfer, and probing molecular chirality using Exciton Coupled Circular Dichroism.

cytochromes and enzymes that are known today belong to the family of cytochrome c in which the heme unit is covalently connected to the polypeptide chain *via* formation of two thioether bonds between two cysteine residues and the vinyl side-chains of the porphyrin ring. The two cysteine residues form a typical amino acid sequence motif CXXCH, which indicates heme c ligation. Some cytochromes have three or four residues between the two cysteines.[1,2] Although the first c-type cytochromes were found in aerobic or facultative anaerobic organisms, these proteins are present in anaerobes in an appreciable diversity.[4a,b] The first cytochromes that were identified, consisted of fewer heme co-factors but a survey of the currently available genomic sequences disclosed that the number of such co-factors per multiheme cytochrome c varies significantly. Two, three, and four are the most common numbers, followed by sequences containing five, eight or ten binding motifs.[1–3] The protein structure with the maximum number of hemes per polypeptide is a hexadecaheme cytochrome,[4c] however, genes coding for polypeptide chains containing 43 and 45 heme binding motifs have been identified in *Geobacter uraniumreducens* and *Anaeromyxobacter dehalogenans*, respectively.[2b] Almost all major groups of bacteria and archaea have multiheme cytochrome c. In some of these organisms, such as representatives of *Geobacter*, *Shewanella*, *Anaeromyxobacter* or *Desulfovibrio* genera, multiheme cytochromes are present in very large numbers that correspond to a high percentage of their proteome, leading to the creation of the term 'cytochromome'.[1,2]

The multiheme c cytochromes and enzymes form families that are recognizably different from the monoheme c cytochromes.[1–3] They are characterized by a low amino acid residue to heme ratio and bis-histidine coordination, with few exceptions. The relative heme arrangements in these multiheme cytochromes are critical for their functional properties and each redox center can be tuned to be active at a different reduction potential thereby allowing a larger range of redox activity. In contrast, proteins with a single redox center have a range of redox activity restricted by the Nernst curve. Various factors are, however, there to influence the reduction potentials of hemes thereby allowing them to be tuned over a wide range. The relevant factors are: the heme environment (namely charges of amino acids, dipoles and exposure to solvents), the nature and relative orientations of the axial ligands, distortions of the porphyrin macrocycle, thermodynamic proton coupling (redox-Bohr effect), and heme–heme interactions.[1–4]

Among all the structures of multiheme proteins reported to date, a conspicuous feature is that the hemes are found clustered in structural arrangements.[1–3] Certainly, these multiheme proteins have majority of their heme units closely packed forming diheme packing motifs with the two heme planes either parallel but offset ('heme stacking motif') or perpendicular to each other ('diheme elbow motif'); Fig. 1–4 demonstrate some representative examples.[1–3,5] The inter-heme iron distances in the parallel motif are around 10 Å and the heme planes are separated by a distance of less than 4 Å

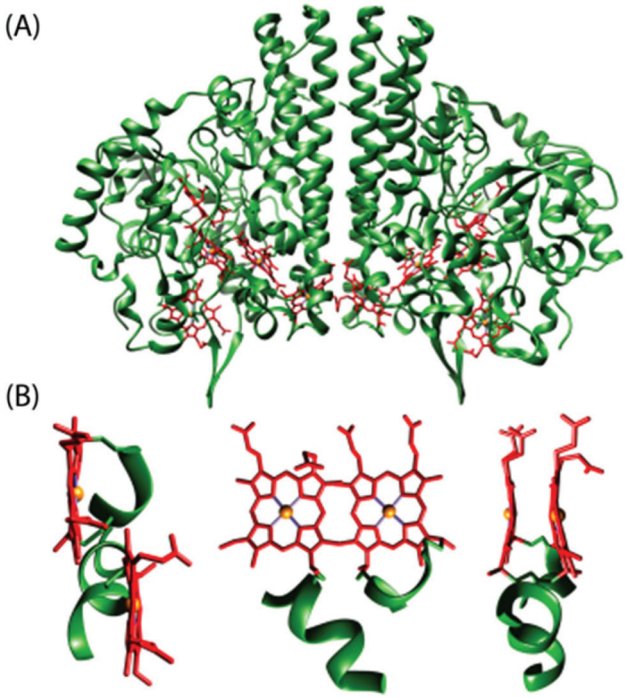

Fig. 1 (A) Structure of cytochrome c nitrite reductase (PDB code 1QDB)[5a] in which the protein chain and the heme groups have been colored green and red, respectively. (B) Different views of the diheme motif formed by heme 3 and heme 4 in the nitrite reductase.

while the heme iron distances in the perpendicular motif are around 12 Å.[1j] Moreover, these diheme motifs form almost superimposable, larger structural heme motifs and the similarity may also extend to the folding of the polypeptide chain surrounding the hemes. Although the functional importance of the spatial disposition of these heme centers is not yet understood, they possibly reveal favorable arrangements to regulate the heme redox potential and/or permit very fast electron transfer. Understanding the importance of these structural arrangements is critical for the interpretation of the functional properties of multiheme cytochrome c which is, however, complicated by the presence of a large number and efficient coupling of the individual heme centers thereby masking their individual properties.[1–3,5] The structural, thermodynamic, and kinetic study of some of the multiheme cytochromes have also been reviewed in recent times.[1]

1.2 Diheme cytochromes

A simplest member of the multi-heme family is the diheme cytochrome c (DHC2) from *G. sulfurreducens*, which has two spectroscopically different heme groups, having different redox properties, attached through a single polypeptide chain.[5c] The heme groups are covalently connected to the protein *via* thioether bonds to cysteine side chains with the sequence C–X_1–X_2–C–H. Fig. 3 shows the stereo view of the overall structure of DHC2 and arrangements of two heme groups therein.[5c] An Fe···Fe distance of 9.4 Å has been

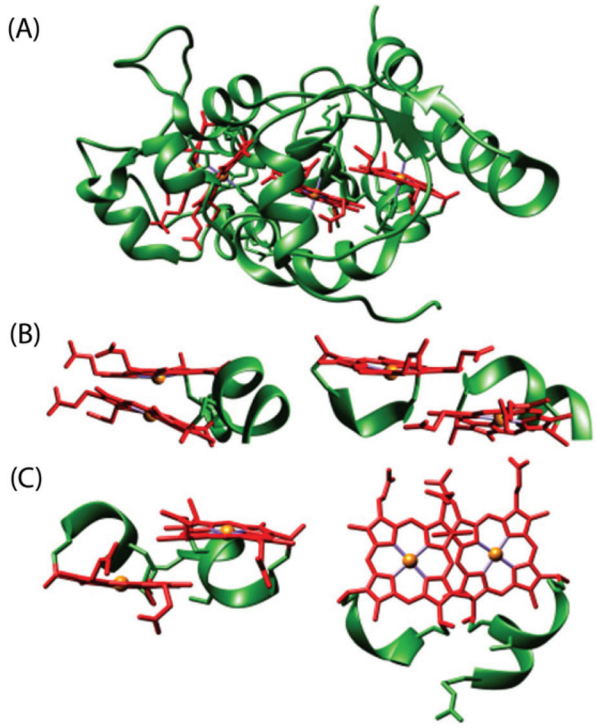

Fig. 2 (A) Structure of the oxidized state of tetraheme cytochrome c554 from *Nitrosomonas europaea* (PDB code 1FT5).[5b] The protein chain and the heme groups have been colored green and red, respectively. Different views of the diheme motifs formed by (B) hemes I and III and (C) hemes II and IV.

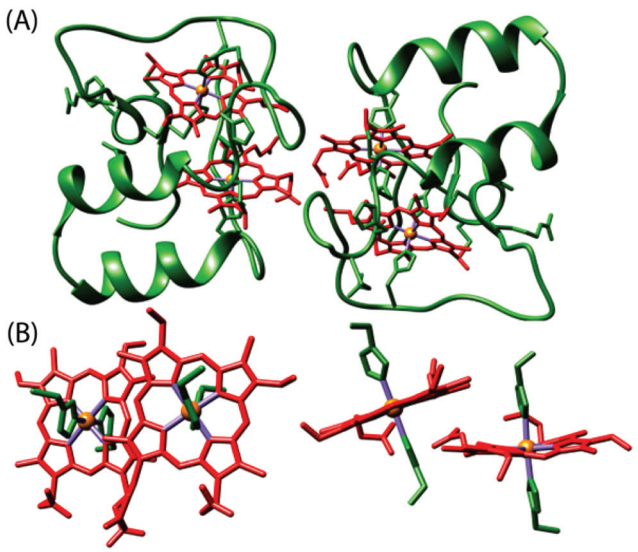

Fig. 3 (A) Structure of the diheme cytochrome c, DHC2, from *Geobacter sulfurreducens* (PDB code 2CZS)[5c] containing 2 monomers per asymmetric unit. Each monomer has two heme groups covalently attached to the protein chain. The protein chain and the heme groups have been colored green and red, respectively. (B) Different views of structural arrangements of the heme groups.

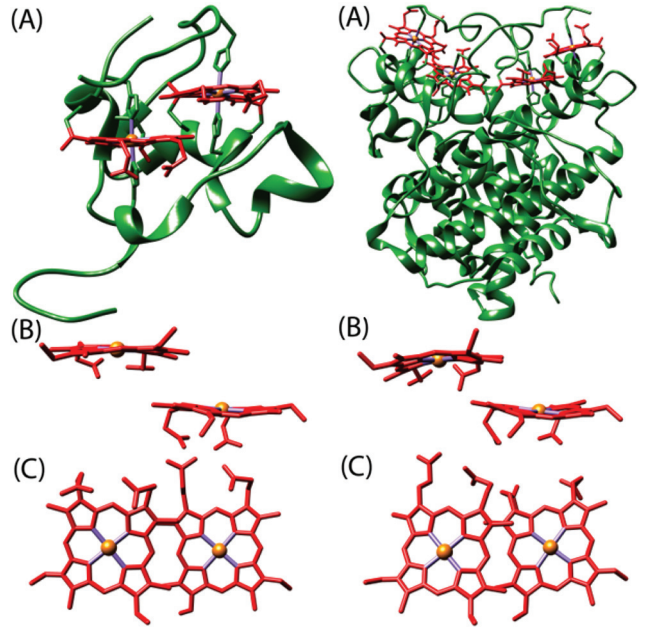

Fig. 4 Left, (A) structure of the diheme cytochrome c, NapB, from *Haemophilus influenzae* (PDB code 1JNI);[3f] (B) side and (C) top views of diheme motifs therein. Right, (A) structure of the aerobic form of the split-Soret diheme cytochrome c from *Desulfovibrio desulfuricans* ATCC 27774 (PDB code 1H21);[3h] (B) side and (C) top views of diheme motifs therein. The protein chain and the heme groups have been colored green and red, respectively.

observed which, however, results in an efficient coupling between two heme centers. The imidazole planes have an interplanar angle of 36° in the axial histidine ligands of heme group I, whereas imidazoles in heme group II are nearly coplanar. Moreover, the porphyrin macrocycle of heme group II is strongly ruffle-distorted while the macrocycle of heme group I is nearly planar. The observed differences in the axial ligand orientations and porphyrin ring deformations between two heme centers in DHC2 [5c] have been proposed to be the consequences of heme–heme interactions. Another diheme cytochrome c with a similar heme arrangement as of DHC2 is the small subunit (NapB) of the periplasmic nitrate reductase (Fig. 4) from *Haemophilus influenzae*.[3f] Here, the two heme groups are nearly parallel and stacked at the van der Waals distances with an Fe···Fe distance of 9.9 Å, similar to the split-Soret diheme cytochrome c (Fig. 4) from *Desulfovibrio desulfuricans* ATCC 27774.[3h]

The structural and functional uniqueness of the di/multiheme cytochromes has inspired us to investigate the effect of inter-heme interactions at the molecular level. The sheer decline in intramolecular interactions with distance makes close proximity of the redox centers indispensable to significantly modify their intrinsic properties.[1d] However, the studies of structure–function relationships of heme proteins are complicated by the presence of huge protein chains. Synthetic chemists, therefore, have been engaged in studying metalloporphyrins *in vitro*, unencumbered by any biological superstructure, which eventually provide convenient systems

for testing various mechanistic hypotheses regarding the fundamental processes. These attractive features have prompted us to thoroughly investigate the structure, function, and properties of the diheme and related complexes as a part of our ongoing research activities.[6–13]

This Perspective documents our endeavor and progress in the investigation of the dihemes and the outcome of the heme–heme interaction operational therein. In the subsequent sections, we will discuss the logical design and the conformational flexibility of the synthetic model of diheme centers followed by the illustration of the heme–heme interaction in the form of alteration of ligand field strength, spin state variation and redox potential modulation, and finally the usefulness of such diheme architectures in dioxygen activation.

2. Ethane-bridged porphyrin dimer as a model of diheme proteins

In order to mimic the heme centers in diheme cytochrome c (DHC2), a covalently linked porphyrin dimer with a highly flexible ethane spacer has been used in which two porphyrin rings can take conformations that are widely seen in the dihemes. Such a porphyrin dimer has been synthesized from the *meso*-formyl-octaethylporphyrinatonickel(II) upon reduction with $NaBH_4$ and subsequent self condensation in *N*,*N*-dimethylformamide using concentrated sulfuric acid as the catalyst.[14] Interestingly, the Fe···Fe non-bonding distances observed in such a model diheme range from 9.39–10.10 Å (*vide infra*),[7–9] which are also very close to the Fe···Fe distances of 9.4 and 9.9 Å observed in the diheme cytochromes isolated from *Geobacter sulfurreducens* and *Haemophilus influenza*, respectively. The similar iron-to-iron distance and heme structural arrangement makes the ethane-bridged porphyrin dimer an ideal choice (Fig. 5) for exploring different aspects of heme–heme interactions in dihemes.

2.1 Conformational flexibility

The conformational variations of porphyrinoids are known to modulate a wide variety of chemical, physicochemical and spectral properties.[15] The supple ethane linker allows an easy interconversion between the *syn* and *anti* conformations (Scheme 1) of the porphyrin dimer triggered by axial ligation, π–π interaction, oxidation/reduction, and treatment with acids/bases. UV-visible spectra can be used as a powerful tool to determine the conformation of the complexes in solution.[6,16] Splitting of the Soret band into two well-resolved transitions, where the low energy transition is assigned to the transition dipole moment running through the 5,15-*meso* carbons ($B_{||}$) and the high energy transition is associated with the transition dipole moment running through the 10,20-*meso* carbons ($B_{\perp}$), is in good agreement with Kasha's exciton coupling theory[17] and is associated with the *anti*-form of the complex in solution.

As displayed in Scheme 1, the ethane-bridged porphyrin dimer is known to switch between the *syn* and *anti* form induced by the external stimuli.[6] It has been found that the free-base ligand and its Zn and cobalt complexes adopt a *syn* conformation in a variety of solvents due to strong π–π interactions between the two rings.[6] Apart from axial ligation, strong π–π interactions between the porphyrin and π-electron rich systems (*e.g.* perylene) lead to the conversion of the *syn* to *anti* form. Fig. 6 shows the molecular structures of the zinc analog in *syn* and *anti* (upon axial coordination of 4-cyanopyridine) forms along with their UV-visible spectra. A split in the Soret band is the indication of *anti*-conformation. Moreover, *syn–anti* conformational switching can also be triggered by the step-wise addition/removal of electrons as depicted in Scheme 2.[6b]

2.2 Model diheme centers

2.2.1 Anionic axial ligand. In an effort to assess the structure–function correlation using the ethane-bridged

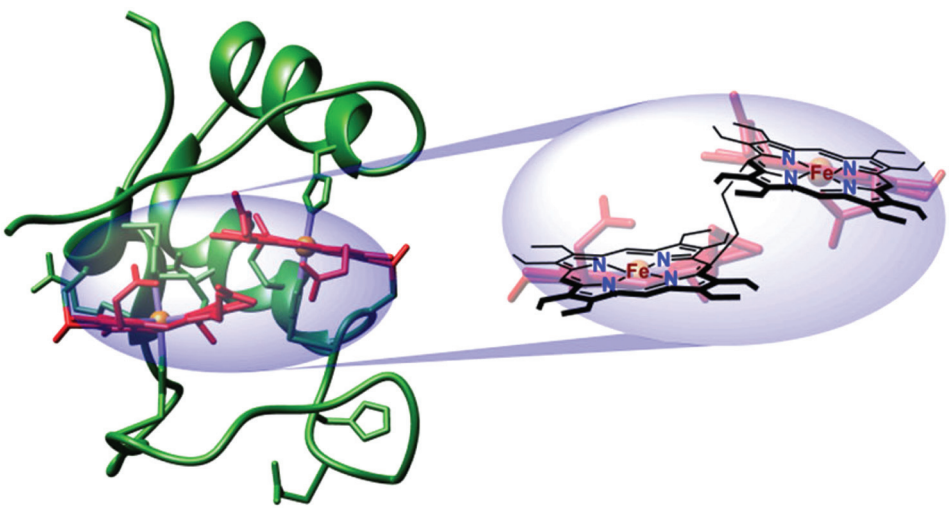

Fig. 5 A schematic diagram overlaying the diheme cytochrome c (DHC2) with the model ethane-bridged diheme architecture.

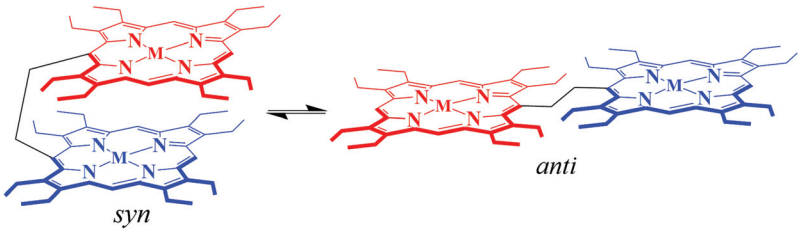

Scheme 1

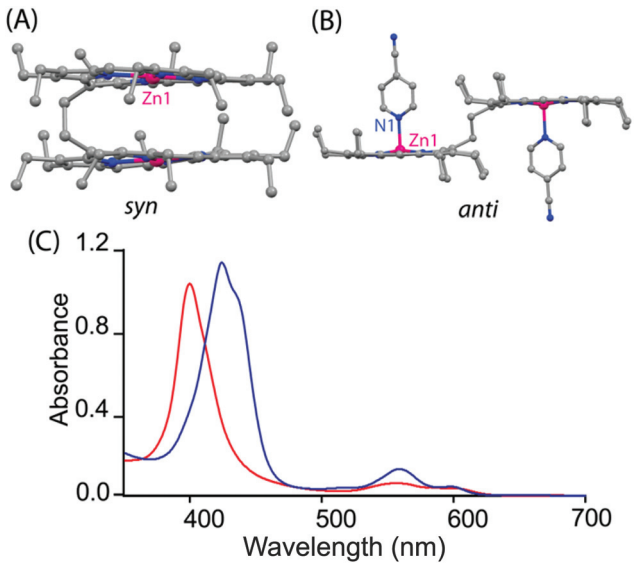

Fig. 6 Molecular structures of (A) the Zn(II) ethane-bridged porphyrin dimer[18] in the *syn* form and (B) its 1 : 2 complex in the *anti* form with 4-cyanopyridine showing all non-hydrogen atoms, (C) UV-visible spectra in chloroform of the Zn(II) ethane-bridged porphyrin dimer in the *syn* form (red line) and the 1 : 2 *anti* form (blue line) with 4-cyanopyridine at 295 K.

porphyrin dimer as a model for diheme centers, a series of *anti*-diiron(III)bisporphyrin **1**·X (X: Cl, Br, I, ClO_4 and SO_3CF_3) have been synthesized (Scheme 3).[7,19] All the complexes have been spectroscopically characterized and two of them (with X = ClO_4 and SO_3CF_3) are also structurally characterized. While all the complexes are found to stabilize the high-spin (S = 5/2) state of iron, the complex with the SO_3CF_3 axial ligand is in a purely intermediate spin (S = 3/2) state. Also, Fe···Fe separations are found to be 10.03 and 9.77 Å, respectively, for the Fe(III) porphyrin dimers with ClO_4 and SO_3CF_3 axial ligands.

Structural parameters such as the displacement of the iron from the mean plane of the $C_{20}N_4$ porphyrinato core (Fe···Ct_p) and the average Fe–Np distance are very characteristics of the iron spin states. For a typical high-spin complex, the Fe–Np and Fe···Ct_p distances are ≥2.045 and ≥0.42 Å, respectively, whereas values reported for spin-admixed complexes are in the range of 1.961–2.038 Å for Fe–Np and 0.10–0.36 Å for Fe···Ct_p, depending on the exact amount of S = 3/2,5/2 character present.[7,20] From the X-ray structural parameters of the iron(III) porphyrin dimer with perchlorate and triflate as axial ligands, a high and intermediate-spin state of iron, respectively, has been assigned. However, porphyrin macrocycles are much more distorted in **1**·SO_3CF_3 compared to **1**·ClO_4.[7a]

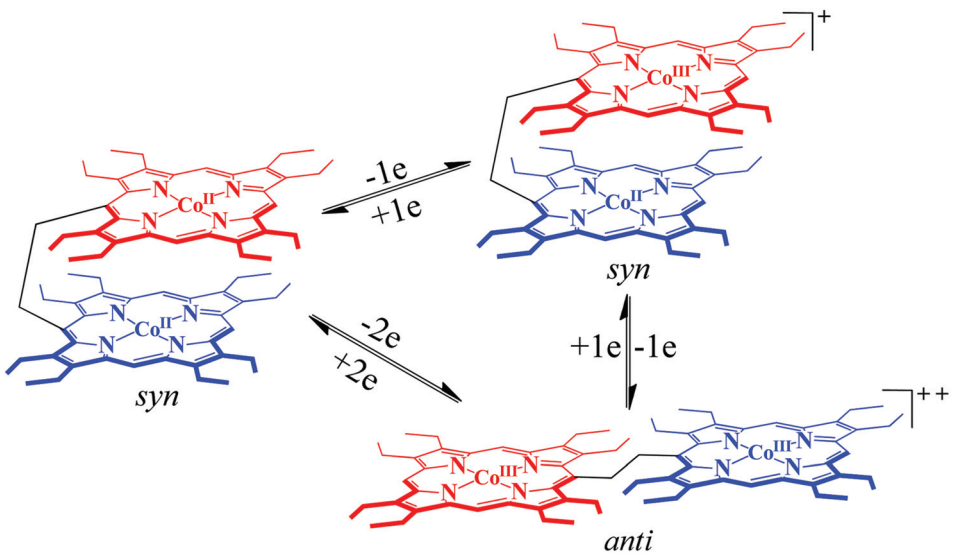

Scheme 2

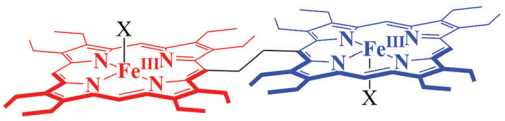

1·X

X = Cl, Br, I, ClO_4 and SO_3CF_3

Scheme 3

It would be interesting to compare the X-ray structure and geometrical parameters of the iron(III) porphyrin dimers with those of monoporphyrin analogs. In the dimeric complex **1**·ClO_4, the Fe–Np and Fe···Ct_p distances are, respectively, 2.062(9) and 0.50 Å (for core-I) and 2.057(9) Å and 0.48 Å (for core-II) while the corresponding Fe–O distances are 1.873(9) and 1.940(7) Å.[7b] In contrast, the monomeric analog Fe^{III}(OEP)-ClO_4 has provided the Fe–Np, Fe···Ct_p and Fe–$OClO_3$ distances of 1.994(10), 0.26 and 2.067(9) Å, respectively.[21a] Thus, while **1**·ClO_4 is a typical high-spin (S = 5/2) complex, its monomeric analog stabilizes the intermediate spin (S = 3/2) state of iron. The porphyrin ring has been found to be highly distorted in the dimeric complex (Fig. 7).

Fig. 8 also displays the X-ray structures and out-of-plane displacement plots of **1**·SO_3CF_3 [7a] and its monomeric counterpart Fe^{III}(OEP)(SO_3CF_3).[21b] For **1**·SO_3CF_3, the Fe–Np and Fe···Ct_p distances are 1.978(3) Å and 0.26 Å, respectively, while the distances of 1.999(2) and 0.22 Å are observed for the monomeric complex, which suggests an intermediate spin (S = 3/2) state of iron for both the complexes. Moreover, Fe–SO_3CF_3 distances of 2.066(3) and 2.0392(14) have been reported for dimeric and monomeric complexes, respectively. As can be seen, porphyrin ring deformation is more in the dimeric complex compared to that in the monomeric analog.

The molecular structures of the complexes in solution are obtained from their ^{1}H NMR spectra. The chemical shifts of

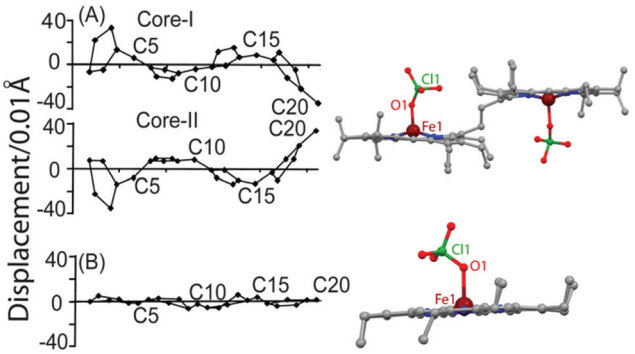

Fig. 7 Out-of-plane displacements (in units of 0.01 Å) of the porphyrin core atoms of (A) **1**·ClO_4 and (B) Fe^{III}(OEP)ClO_4 [21a] from the mean plane of the $C_{20}N_4$ porphyrinato core. The horizontal axis shows the bond connectivity between atoms. Molecular structures (at 100 K) of the corresponding complexes showing all non-hydrogen atoms are given on the right.

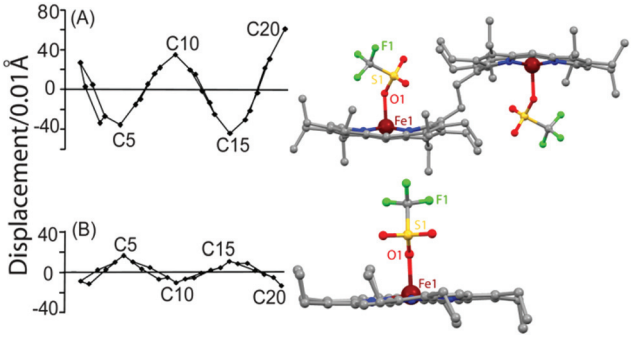

Fig. 8 Out-of-plane displacements (in units of 0.01 Å) of the porphyrin core atoms of (A) **1**·SO_3CF_3 and (B) Fe^{III}(OEP)(SO_3CF_3)[21b] from the mean plane of the $C_{20}N_4$ porphyrinato core. The horizontal axis shows the bond connectivity between atoms. Molecular structures (at 100 K) of the corresponding complexes showing all non-hydrogen atoms are given on the right.

the methylene, methyl and *meso* protons are highly sensitive to the spin states. For a typical five-coordinate high-spin Fe(III) complex with an OEP-type ligand, –CH_2 proton signals are shifted downfield to ~+40 ppm (average) while the *meso* protons appear at the far upfield to ~–60 ppm (average). As iron moves towards the porphyrin mean plane in spin-admixed complexes, *meso* proton signals move more and more downfield while –CH_2 protons move upfield. It has also been found that the high-spin complexes exhibit –CH_3 signals more downfield than the complexes with intermediate spin as the unpaired spins can be delocalized up to –CH_3 through σ-bonds in the former.

Fig. 9 shows the ^{1}H NMR spectra of **1**·ClO_4 and **1**·SO_3CF_3. The highly downfield shifted methylene (34.0 to 58.9 ppm) and bridging –CH_2 (64.5 ppm) resonances as well as the highly upfield shifted *meso* proton signals (–35.2 to –52.4 ppm) clearly indicate the presence of a high-spin (S = 5/2) Fe(III) center in **1**·ClO_4. In contrast, the ^{1}H NMR of its monomeric analog Fe^{III}(OEP)ClO_4 shows a downfield shifted methylene proton signal at 35.5 ppm and an upfield shifted *meso* proton signal at –5.5 ppm, which indicates an intermediate-spin state (S = 3/2) of Fe(III).[21c] In **1**·SO_3CF_3, however, eight sharp methylene peaks have been observed in the relatively narrow region (from 16.0 to 21.6 ppm) along with two sharp *meso* resonances at –3.7 and –15.6 ppm indicating a pure intermediate state (S = 3/2) of Fe(III). In contrast, two downfield shifted methylene resonances (at 34.6 and 49.4 ppm) and an upfield shifted *meso* resonance (–24.6 ppm) suggest the presence of a nearly admixed high-spin Fe(III) center in Fe^{III}(OEP)(SO_3CF_3), the monoheme analog of **1**·SO_3CF_3.[21c] The spin states of iron have been further confirmed by EPR and magnetic susceptibility measurements of the polycrystalline samples also. Thus, as observed in solid, iron(III) porphyrin dimers with perchlorate and triflate as axial ligands stabilize a high and intermediate-spin of iron, respectively, which is, however, opposite to what has been expected for the monomeric complex.

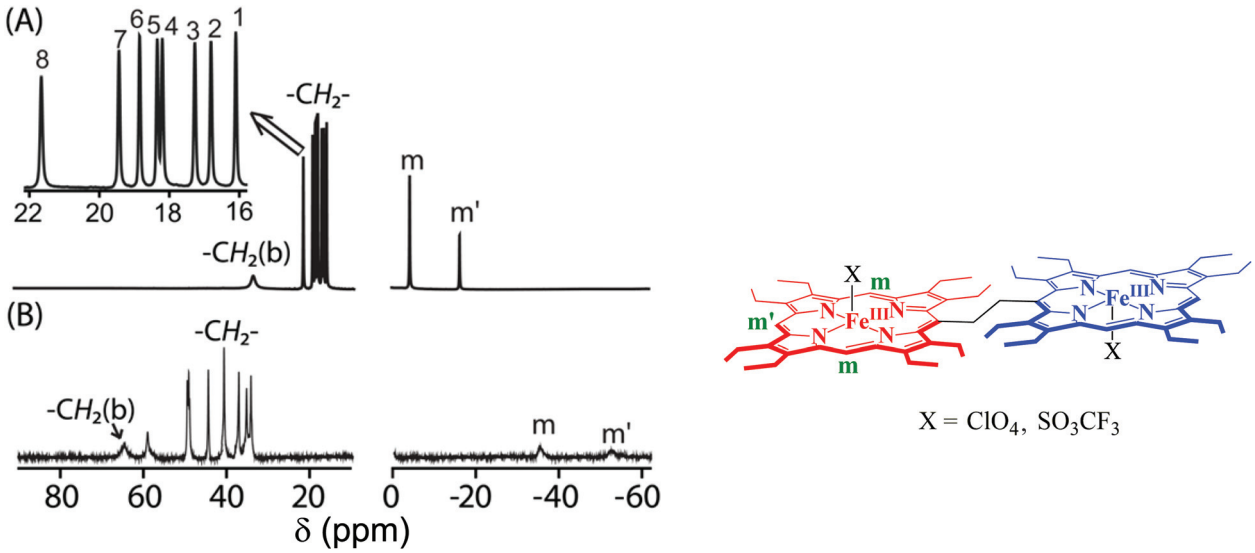

Fig. 9 ^{1}H NMR spectra (in $CDCl_3$ at 295 K) of (A) **1**·SO_3CF_3 and (B) **1**·ClO_4.

The factors that affect the conversion from the high-spin to an intermediate-spin state deserve comment. Studies on the model heme complexes suggest that a weak field axial ligand (*e.g.* ClO_4^-) stabilizes the intermediate-spin state of Fe(III) while $CF_3SO_3^-$ forms a mostly admixed high-spin complex.[20,21] However, the porphyrin ring deformation is also known to play an important role in controlling the spins of iron(III) while a large deformation favours stabilization of an intermediate spin state.[20] The porphyrin ring in **1**·SO_3CF_3 has been found to be more ruffle-distorted compared to **1**·ClO_4. The ruffling of the porphyrin ring affects the energy level of d orbitals; the d_{xy} orbital is destabilized due to its interaction with the a_{2u} orbital of porphyrin, while the contraction of the equatorial Fe–Np bonds destabilizes the $d_{x^2-y^2}$ orbitals which are, in fact, responsible for the stabilization of the pure intermediate spin of iron in **1**·SO_3CF_3.[7a] In contrast, the destabilization of the d_{xy} and $d_{x^2-y^2}$ orbitals in **1**·ClO_4 is not sufficient enough for such a change in the spin state. Thus, while **1**·ClO_4 is a typical high-spin complex, the larger size of the triflate induces greater ruffling of the porphyrin macrocycle resulting in the stabilization of pure intermediate-spin in **1**·SO_3CF_3 although according to the axial ligand strengths ('magnetochemical series'[22]) reverse order of spin stabilization was expected.[7a] Thus, the complete reversal of the ligand field strength between ClO_4^- and $CF_3SO_3^-$ in the magnetochemical series has been obtained using a bisporphyrin framework.[7a]

2.2.2 Axial phenoxide coordination. Instigated by the interesting results, we undertook further investigation using a variety of axial ligands in order to understand the effects of heme–heme interactions on the individual heme centers. Therefore, a series of diiron(III)bisporphyrin complexes with axial phenoxide coordination (Scheme 4) have been investigated and their structures and properties are compared with the corresponding monoporphyrin analogs.[8] The complexes

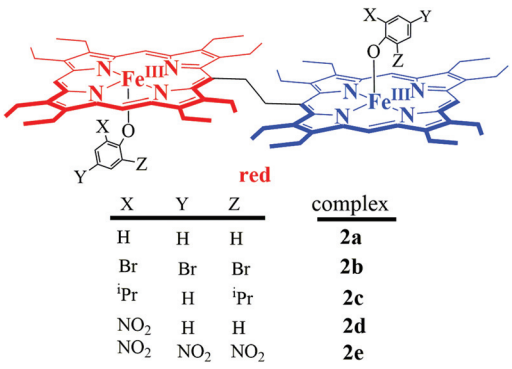

X	Y	Z	complex
H	H	H	**2a**
Br	Br	Br	**2b**
^{i}Pr	H	^{i}Pr	**2c**
NO_2	H	H	**2d**
NO_2	NO_2	NO_2	**2e**

Scheme 4

have been successfully characterized including single crystal X-ray structure determinations. Fig. 10 compares the structure of **2e** and its monomeric counterpart Fe^{III}(OEP){O-2,4,6-$(NO_2)_3C_6H_2$}.

The average Fe–Np distances are in the range of 2.057 to 2.077 Å and the Fe···Ct_p lies within the value of 0.51 to 0.56 Å for complexes **2a**, **2b**, and **2c**, which indicate the presence of a high-spin Fe(III) center in the complexes. However, **2e** has an average Fe–Np distance of 1.972(3) Å, the shortest among all the phenolato complexes reported so far, while the Fe···Ct_p distance is 0.23 Å suggesting a pure intermediate-spin Fe(III) center. In sharp contrast, the average Fe–Np and Fe···Ct_p distances for Fe^{III}(OEP){O-2,4,6-$(NO_2)_3C_6H_2$} (which is the monoporphyrin analog of **2e**) are 2.049(2) and 0.40 Å, respectively, which confirms the stabilization of the high-spin state.[8a] Also, Fe···Fe separation within the molecules in the dimeric complexes varies within the range of 9.40 to 10.10 Å. The room temperature Mössbauer parameters of **2b** [δ (ΔE_q): 0.28 (0.66)

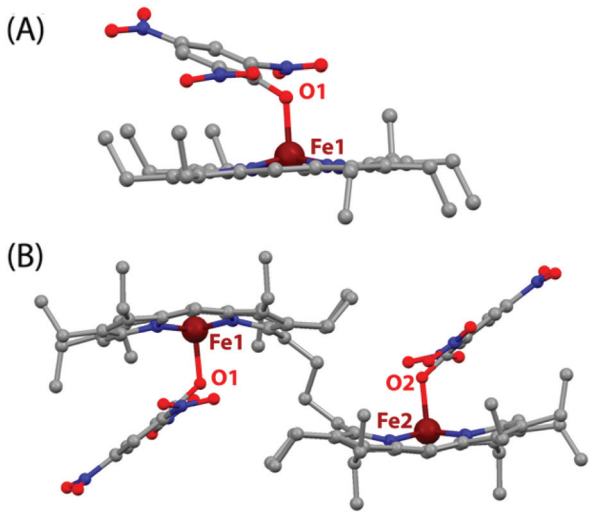

Fig. 10 Molecular structures (at 100 K) of (A) Fe^{III}(OEP){O-2,4,6-$(NO_2)_3C_6H_2$} and (B) **2e** showing all non-hydrogen atoms.

mm s^{-1}] and **2e** [δ (ΔE_q): 0.27 (2.7) mm s^{-1}] also support the Fe(III) spin states as indicated by the X-ray structure of the complexes.[8a]

Fe–Np and Fe–O distances of 1.972(3) Å and 2.000(2) Å, observed for **2e**, are the shortest and longest distances, respectively, in the series. Interestingly, **2e** is the first phenoxide coordinated Fe(III)porphyrin having a pure intermediate state of iron while all other complexes stabilize in the high-spin state only.[8,23] Also, the binding of 2,4,6-trinitrophenol to the iron(III) monoporphyrin, Fe^{III}(OEP){O-2,4,6-$(NO_2)_3C_6H_2$}, stabilizes the high-spin state of iron.[8a] Among all the phenolato complexes, the porphyrin ring is most distorted in **2e** while Fe^{III}(OEP)-{O-2,4,6-$(NO_2)_3C_6H_2$}, which is the monomeric analog of **2e**, shows a nearly planar porphyrin core (Fig. 11).[8a] The large increase in ring deformation in **2e**, compared to its monomeric analog, is a result of the heme–heme interactions in dihemes, which eventually results in the stabilization of the intermediate-spin state of Fe(III).

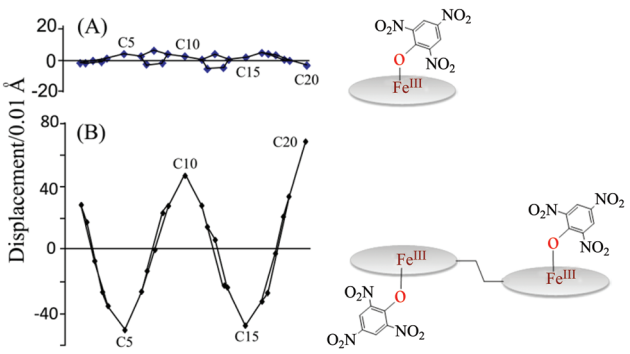

Fig. 11 Out-of-plane displacements (in units of 0.01 Å) of the porphyrin core atoms of (A) Fe^{III}(OEP){O-2,4,6-$(NO_2)_3C_6H_2$} and (B) **2e** from the mean plane of the $C_{20}N_4$ porphyrinato core.

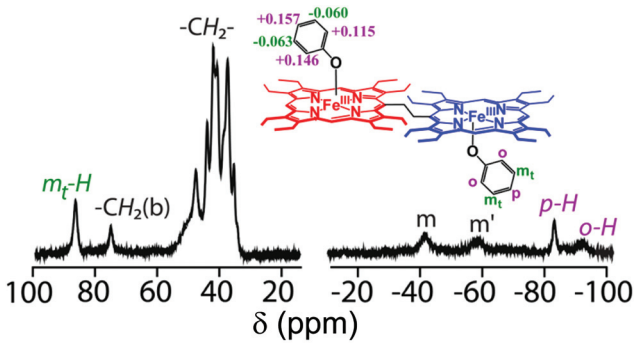

Fig. 12 ^{1}H NMR spectrum (in $CDCl_3$ at 295 K) of **2a**; inset shows the Mulliken spin densities and the proton-numbering scheme on phenolato carbons.

The nature and positioning of methylene and *meso* proton signals in the ^{1}H NMR spectra of complexes **2a** to **2d** confirm the high-spin (S = 5/2) state of Fe(III) in the complexes in solution. In **2e**, however, the ^{1}H NMR spectrum suggests the presence of an intermediate-spin Fe(III) center in solution as was also observed in the solid.[8a] The phenolato resonances (Fig. 12) are, however, shifted to both upfield and downfield regions in the ^{1}H NMR spectra which have been rationalized on the basis of Mulliken spin density calculation. Positive spin densities at the *ortho*- and *para*-carbons of the phenolato ring result in upfield shifting of the corresponding protons, while a negative spin density at the *meta*-position has an opposite effect. The alternating signs of spin densities at the *ortho*-, *meta*-, and *para*-carbons are also indicative of π-spin delocalization from the Fe(III) center to the phenolato ligand.[8a]

Fig. 13 compares the ^{1}H NMR spectra of **2e** along with its monoporphyrin analogs: Fe^{III}(OEP){O-2,4,6-$(NO_2)_3C_6H_2$} and Fe^{III}(Me-OEP){O-2,4,6-$(NO_2)_3C_6H_2$}.[8a] Traces B and C show the ^{1}H NMR spectra of Fe^{III}(Me-OEP){O-2,4,6-$(NO_2)_3C_6H_2$} and Fe^{III}(OEP){O-2,4,6-$(NO_2)_3C_6H_2$}, respectively, and, as can be seen, the nature and position of the methylene and *meso* resonances are characteristics of the pure high-spin state of Fe(III) in the complexes. Trace A, however, shows the spectra of **2e** in which the methylene and *meso* signals have remarkably shifted upfield and downfield, respectively, as compared to their monomeric analogs. Therefore, axial coordination of 2,4,6-trinitrophenol to the corresponding Fe(III) complex of monoporphyrins stabilizes only the pure high-spin state (S = 5/2) while the intermediate-spin state is stabilized in the diheme analog (**2e**). The alteration of the spin state from high-spin to intermediate-spin on moving from Fe^{III}(OEP){O-2,4,6-$(NO_2)_3C_6H_2$} to the diheme analog **2e**, has been attributed to the effect of heme–heme interactions.[8a]

2.2.3 Axial thiophenolate coordination. What followed immediately, is a series of thiophenolato coordinated diiron(III) bisporphyrins along with their monomeric counterparts (Scheme 5).[9]

All the thiophenolato diiron(III)bisporphyrin complexes, shown in Scheme 5, have been structurally characterized.

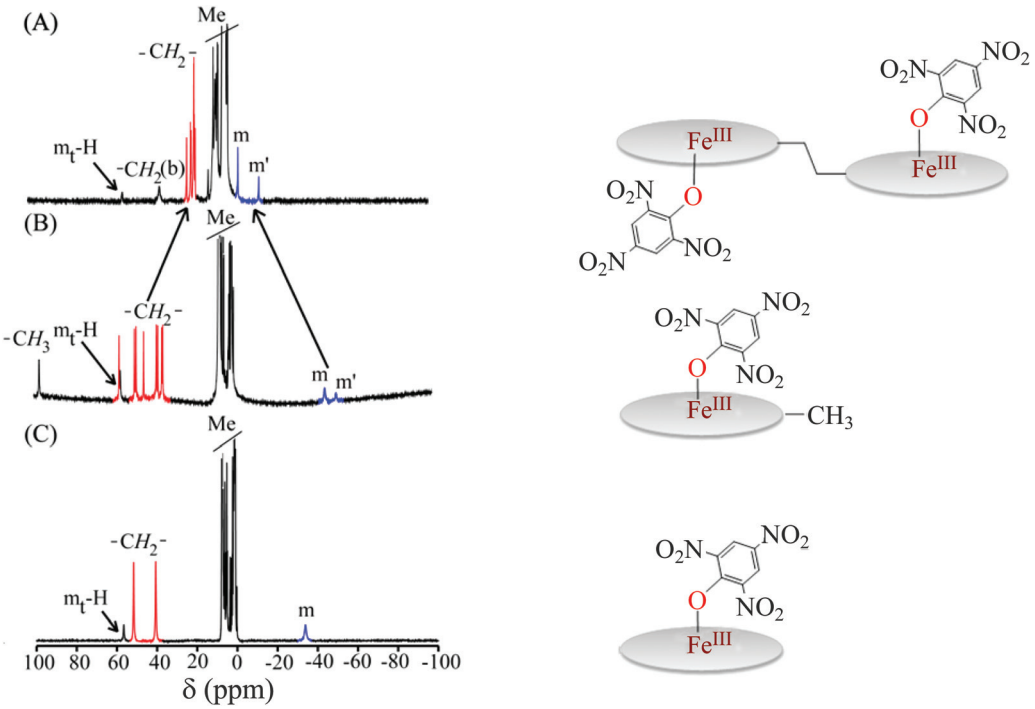

Fig. 13 ^{1}H NMR spectra (at 295 K in $CDCl_3$) of (A) **2e**, (B) Fe^{III}(Me-OEP){O-2,4,6-$(NO_2)_3C_6H_2$} and (C) Fe^{III}(OEP){O-2,4,6-$(NO_2)_3C_6H_2$}.

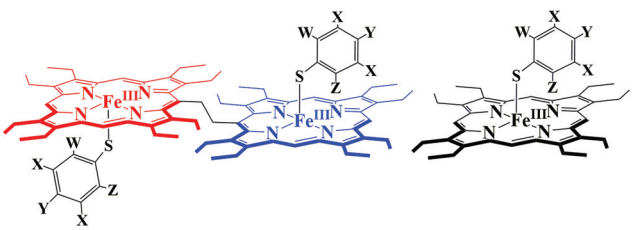

W	X	Y	Z	complex	complex
H	H	H	H	**3a**	**4a**
Me	H	Me	Me	**3b**	**4b**
Cl	H	H	Cl	**3c**	**4c**
F	F	F	F	**3d**	**4d**

Scheme 5

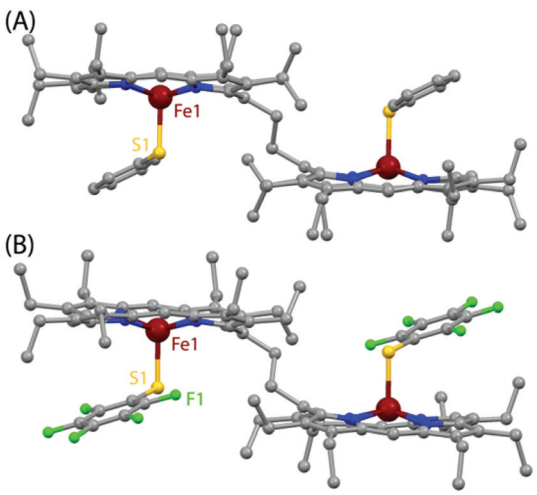

Fig. 14 Molecular structures (at 100 K) of (A) **3a** and (B) **3d** showing all non-hydrogen atoms.

Fig. 14 displays the molecular structures of **3a** and **3d** as two representative cases.[9] The Fe···Fe nonbonding distances within the molecules in the dimeric complexes have been found to vary within the range of 9.46 to 9.76 Å. The average Fe–Np (2.052 to 2.059 Å) and Fe···Ct_p (0.41 to 0.61 Å) distances suggest a high-spin Fe(III) center for all the complexes. The Fe–S bond distances have been found to be dependent on the electron donating/withdrawing nature of the substituent on the thiophenols. The Fe–S bond distances in **3a–3d** are larger compared to the Fe–O distances observed in their phenolato counterparts (*vide supra*). This indicates that thiophenols are weaker donors than phenols. The Fe–S–C angle in the complexes **3a–3d**, though much smaller than the Fe–O–C angles in their phenolato counterparts, is similar to the Fe–S–C angles in the monoporphyrin complexes.

The porphyrin core deformations of the thiophenolato complexes are similar to their phenolato counterparts and can be best appreciated by turning to Fig. 15 where the out-of-plane displacements of the porphyrin core atoms of **3a**, **2a** and **4a** are compared.[9] While the porphyrin macrocycle in thiophenolato and phenolato complexes of the porphyrin dimer is highly distorted, the ring is nearly planar in the corresponding mono-

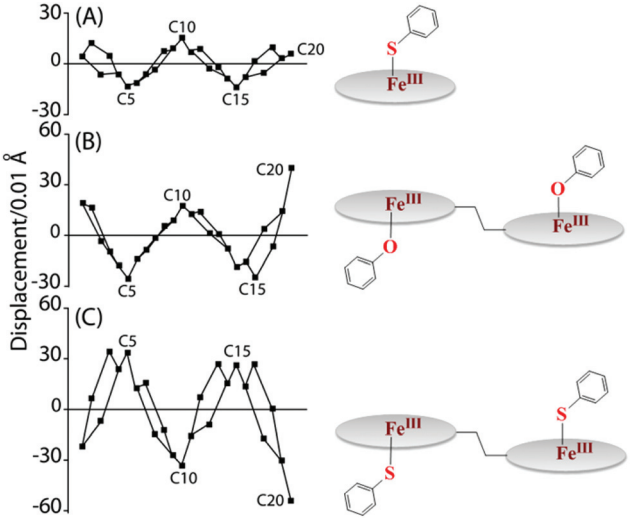

Fig. 15 Out-of-plane displacements (in units of 0.01 Å of the porphyrin core atoms) from the least-squares plane of the $C_{20}N_4$ porphyrinato core of (A) **4a**, (B) **2a**, and (C) **3a**.

meric thiophenolato complex **4a**.[24] The interaction between the two rings in the model diheme results in larger ring deformation of the individual porphyrin centers. It is also interesting to note here that both the average displacement of the porphyrin core atoms and Fe···Ct_p are greater in the thiophenolato complexes compared to the corresponding phenolato complexes of diiron(III)bisporphyrin.

EPR spectra of all the thiophenolato diiron(III)bisporphyrin complexes are axially symmetric with $g_\perp \sim 6.0$ and $g_{II} \sim 2.0$ due to the high-spin ($S = 5/2$) state of iron in the complexes, both in solid and solution phases.[9] The ^{1}H NMR spectra of the complexes (**3a–3d**) are also similar with the related phenolato analogs containing the high-spin state of iron.[9] Similar to the phenolato diiron(III)bisporphyrin complexes, **2a–2e**, the *ortho*- and *para*-protons show upfield shifts in the ^{1}H NMR spectra while *meta*-protons move downfield, which is indicative of π-spin delocalization on the thiophenolato ligand.

Addition of excess thiophenol to the dichloromethane solution of **3** results in the formation of six-coordinate complex **5** (Scheme 6).[9] The complexes, **5a–5d**, produce axial EPR spectra (Fig. 16), which is typical for low-spin complexes at 120 K. It has been proposed that one axial ligand binds as thiophenolate while the other one as thiophenol. However, the formation of such six-coordinate complexes doesn't take place upon the addition of excess phenols to the related phenolato diiron(III) bisporphyrin complexes, **2a–2e**.

2.2.4 Metal redox. Fig. 17 compares the cyclic voltammograms of both five and six-coordinate complexes. The study reveals a large positive shift of the Fe(III)/Fe(II) redox couple for the complexes going from **1**·Cl ($E_{1/2} = -1.34$ V)[7b] to **2a** ($E_{1/2} = -0.92$ V)[8a] to **3a** ($E_{1/2} = -0.76$ V).[9] A single point energy calculation clearly shows that in the HOMO for **2a**, **3a** and **1**·Cl the electron density on the axial ligand decreases as we move from thiophenol to phenol to chloride.[9] This explains the easier

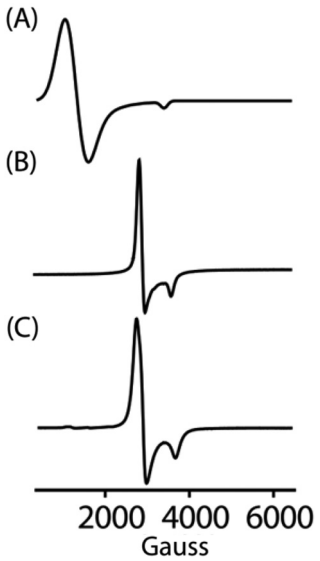

Fig. 16 X-band EPR spectra in CH_2Cl_2 (at 120 K) of (A) **3a**, (B) **5a** and (C) **5b**.

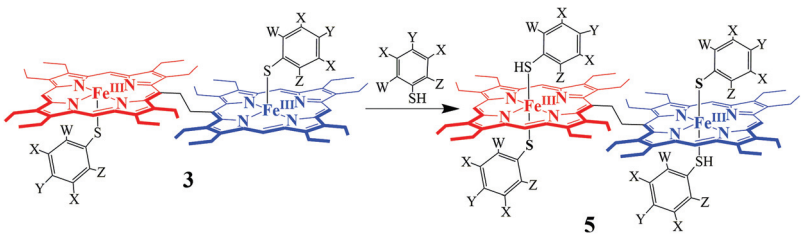

W	X	Y	Z	complex
H	H	H	H	**5a**
Me	H	Me	Me	**5b**
Cl	H	H	Cl	**5c**
F	F	F	F	**5d**

Scheme 6

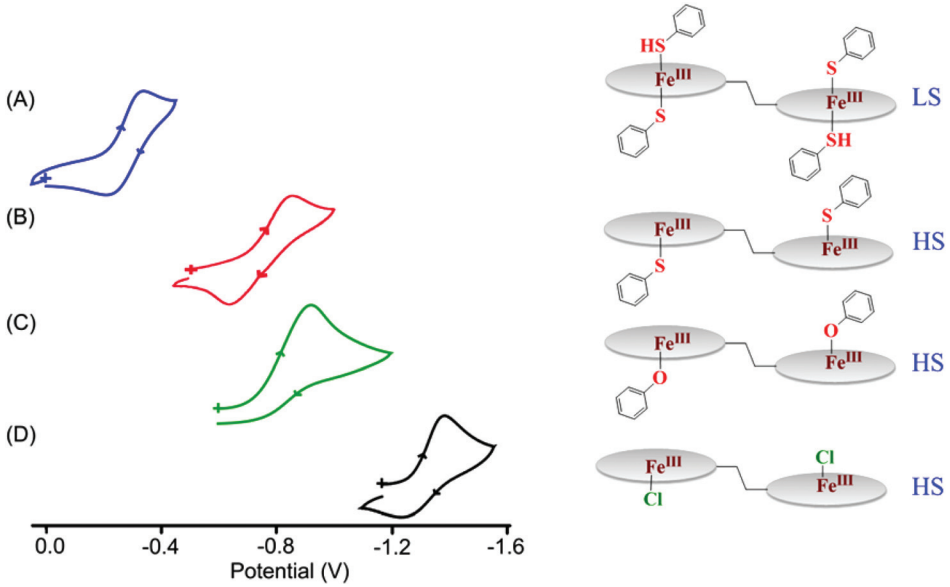

Fig. 17 Fe(III)/Fe(II) redox couple (at 298 K in CH_2Cl_2) of (A) **5a**, (B) **3a**, (C) **2a** and (D) **1**·Cl. The reference electrode was Ag/AgCl.

reduction of the Fe(III) center in the order: $Cl^- < PhO^- < PhS^-$. Thiophenol is a weaker electron-donor than phenol due to back-donation of electron density from the iron center to an empty d-orbital of sulfur.

The Fe(III)/Fe(II) redox potential of the six-coordinate complex, **5a**, was observed at −0.27 V.[9] The large positive shift of 490 mV on moving from the five-coordinate high-spin complex (**3a**) to the six-coordinate low-spin complex (**5a**) suggests easier reduction of the iron center upon thiophenol coordination at the sixth position. Such a positive shift in the Fe(III)/Fe(II) redox potential has been attributed to the contributions from the sixth axial coordination as well as the spin state change from high to low.[8a] As can be seen, a variation of ~1.10 V for the Fe(III)/Fe(II) redox potential can be achieved by the combination of axial coordination and metal spin. The control of heme redox potential by the spin state of iron is a key step in cytochrome P450 catalysis.[25]

A plot of Fe(III)/Fe(II) potential of complexes **3a–3d** and **4a–4d** against pK_a of the corresponding thiophenols (Fig. 18) has revealed a linear relationship.[9] Similar pK_a dependence of the Fe(III)/Fe(II) redox couple has been also observed for the phenolato analogs **2a–2e**, where the deviation of **2e** from linearity was demonstrated in terms of spin state change.[8a,9] It is however interesting to note the steepness of the slope for the diheme complexes **3a–3d** as compared to their monoheme analogs **4a–4d**. A potential window of 540 mV for the Fe(III)/Fe(II) redox couple has been observed in the diheme series **3a–3d** in contrast to the potential window of only 270 mV for the monomeric analogs **4a–4d**. Such an increase in the potential range on going from monoheme to diheme can be attributed to the intermacrocyclic interaction in the dihemes.[9]

The Fe(III)/Fe(II) redox couple has been found to be influenced by various factors including axial coordination, porphyrin ring deformation, change in the metal spin state and

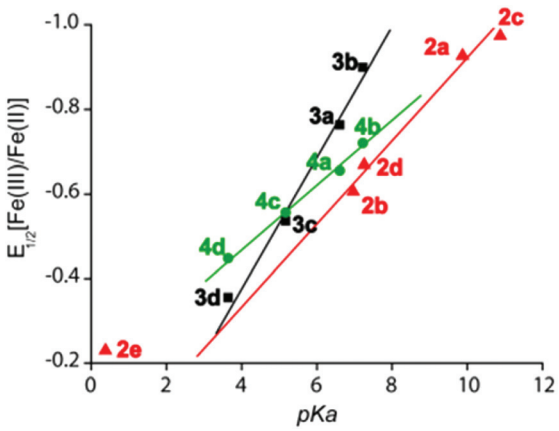

Fig. 18 Plots of pK_a of thiophenol/phenol *vs.* $E_{1/2}$ [Fe(III)/Fe(II)] in V of thiophenolato diiron(III)bisporphyrins (■), phenolato diiron(III)bisporphyrins (▲) and thiophenolato iron(III)monoporphyrins (●).

inter-heme interactions. However, it would be difficult to separate out the individual contributions alone since many of the factors are interrelated. A clear visualization of the outcome of inter-heme interactions can be obtained by comparing the cyclic voltammetric responses of dicobalt(II)bisporphyrin (which is found to be cofacial) and its monomeric analog, $Co^{II}OEP$ (Fig. 19) under identical conditions and in the absence of any axial coordination.[6b] The increased number of oxidative responses, from three to four, in the cyclic voltammograms of dicobalt(II)bisporphyrin as compared to $Co^{II}OEP$ indicates strong through space electronic communication in the complex. One $Co^{II}OEP$ unit of the dimeric complex is oxidized at 0.25 V to generate $Co^{III}OEP$ at a potential much lower than that of monomeric $Co^{II}OEP$ alone which is due to the increased electron density in the bisporphyrin scaffold. The

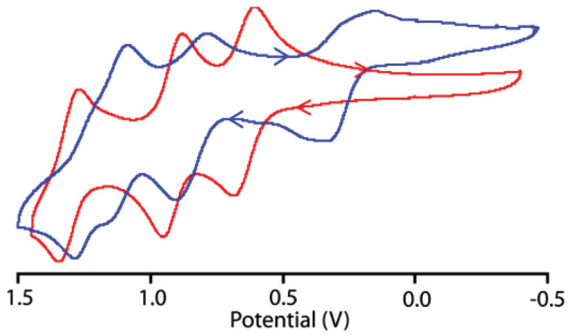

Fig. 19 Comparison between cyclic voltammograms of the Co(II) ethane-bridged porphyrin dimer (blue-line) and monomeric $Co^{II}OEP$ (red-line) in CH_2Cl_2 at 298 K. The reference electrode was Ag/AgCl.

second $Co^{II}OEP$ is then oxidized at a significantly higher potential of 0.83 V due to strong inter-macrocyclic interactions in the dicobalt complex.[6b]

2.3 μ-Oxo dimers

Addition of 5% aq. NaOH solution to the dichloromethane solution of **1**·X changes the color from dark red to green immediately due to the formation of diiron(III)-μ-oxo bisporphyrin, **6a** with a conformational change from *anti* to *syn* (Scheme 7).[7b,10] Such an acid–base controlled conformational switching is also found to be reversible in nature. Similarly, *cis* 1,2-bis[chloroiron(III)5-(2,3,7,8,12,13,17,18-octaethylporphyrinyl]ethene, which also possesses great horizontal and vertical flexibility,[26] transforms to *cis* diiron(III)-μ-oxo bisporphyrin, **6b** (Scheme 7).[10a]

The complex **6a** crystallizes as two different solvates: one with CH_3CN and the other one with toluene, however, both are very similar.[7b,10b] Molecular structures of the complexes are shown in Fig. 20. The Fe–O–Fe unit has been found to be remarkably bent with an angle of 147.9(1)°. There are at least six C···C nonbonding distances (<3.4 Å) between two porphyrin rings which are less than their van der Waals radii; the closest being the two bridging *meso* carbons which are separated by 3.016(5) Å. Strong π–π interactions must have contributed in

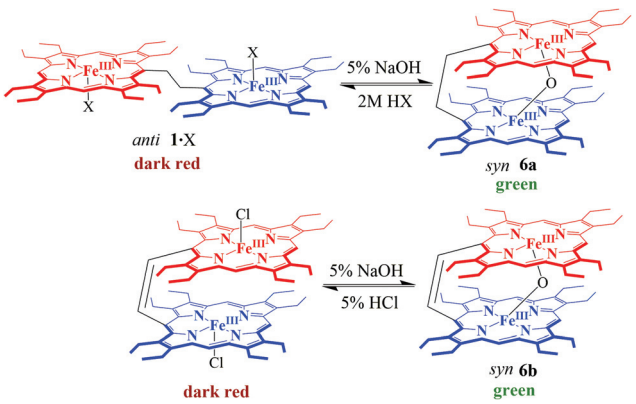

Scheme 7

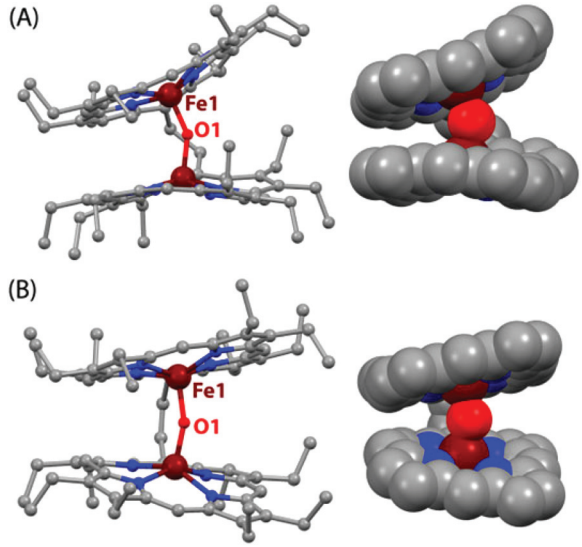

Fig. 20 Molecular structures (at 100 K) of (A) **6a** and (B) **6b** showing all non-hydrogen atoms. Diagrams on the right showing the close contacts between two rings (hydrogen and ethyl groups are omitted for clarity).

the stabilization of highly bent and extremely strained geometry. Structural analysis of **1**·ClO_4 and **6a** reflects a very high vertical flexibility of over 6.5 Å.[7b,10b] However, the rigid alkene spacer in **6b** restricts the rotation of the individual porphyrin cores resulting in a fully eclipsed face-to-face ring orientation with a highly bent Fe–O–Fe unit with an angle of 150.9(2)°.[10a] The porphyrin rings of **6a** and **6b** are highly distorted compared to their unbridged dimer, $[Fe^{III}(OEP)]_2O$,[27] which can be appreciated by referring to Fig. 21. As can be seen, the *meso* carbons (C20) that are connected by the linker are displaced most from the mean porphyrin plane in **6a**/**6b**. Structural parameters of the complexes are compared in Table 1.

Both the Fe(III) centers are high-spin in nature in **6a** and **6b** as reflected in their X-ray structures and also in their Mössbauer spectra. Their ^1H NMR spectra indicate that the *syn* orientation is preserved in solution.[10] The cyclic voltammogram of **6a** recorded at 25 °C in CH_2Cl_2 with 0.1 M tetrabutylammonium perchlorate (TBAP) as the supporting electrolyte and Ag/AgCl as the reference electrode shows four reversible/quasi-reversible one-electron oxidations at 0.57, 0.87, 1.27, and 1.39 V and one reductive response at −1.39 V. Under identical conditions, **6b** also produces a similar voltammetric response; four one electron oxidations at 0.50, 0.84, 1.28 and 1.38 V and one-electron reduction at −1.36 V. It would be interesting to note here that under identical conditions, their unbridged counterpart $[Fe(OEP)]_2O$ shows similar oxidative responses at relatively higher potentials (0.65, 0.93, 1.30, 1.54 V) and reduction at slightly lower potentials (−1.35 V). The presence of two porphyrin macrocycles within a short distance in **6a**/**6b** makes the porphyrin core highly deformed as well as more electron rich that is responsible for its easier oxidations.

The highly strained geometry around oxygen allows **6a** and **6b** to show some unusual reactivity that is not observed in the

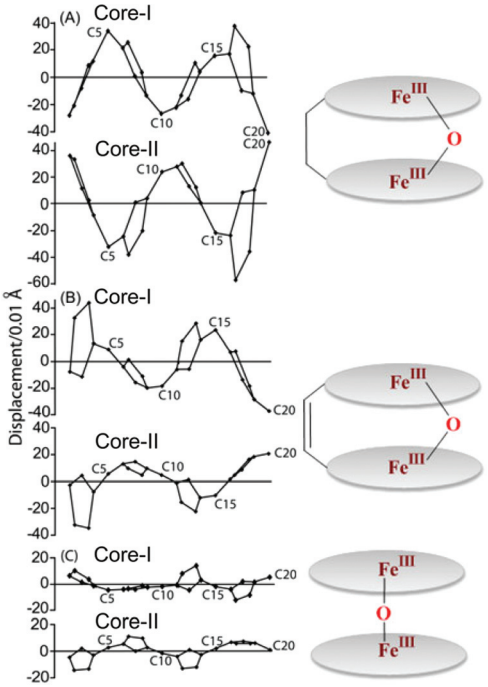

Fig. 21 Out-of-plane displacements (in units of 0.01 Å) of the porphyrin core atoms from the mean porphyrin plane of the $C_{20}N_4$ porphyrinato core of (A) **6a**, (B) **6b** and (c) $[Fe^{III}(OEP)]_2O$[27] (monoclinic).

related unbridged complex $[Fe^{III}(OEP)]_2O$. The complex **6b** upon photoirradiation (λ_{exc} > 365 nm, O–Fe LMCT transition) with excess phosphite in benzene under anaerobic conditions undergoes an immediate change in the absorption spectra (Fig. 22); the peaks corresponding to diiron(III)-μ-oxo bisporphyrin decrease while peaks corresponding to diiron(II)bisporphyrin keep increasing with time.[10a] Moreover, each photoreaction produces a stoichiometric amount of $O{=}P(OR)_3$ and diiron(II)bisporphyrin complex which reforms **6b** in the presence of O_2 to re-enter into the catalytic cycle (Scheme 8). A highly oxidized ferryl intermediate ($PFe^{IV}{=}O$) has been proposed to be responsible for the oxidation of the substrate.[28]

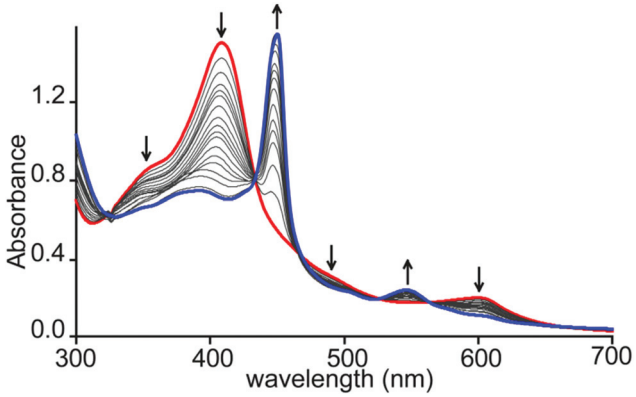

Fig. 22 Time-evolution spectral changes of **6b** (red line) in benzene (~10^{-6} M) in the presence of triethylphosphite (~0.3 M) at 295 K under nitrogen. The arrows indicate the disappearance of **6b** and appearance of diiron(II) bisporphyrin species (blue line).

Similar results are also obtained with **6a** but with less catalytic efficiency.[10b]

2.4 μ-Hydroxo dimers: unusual stabilization of two spin states of iron

Protonation of the diiron(III)-μ-oxo bisporphyrins, **6**, by a strong Brønsted acid with a very weakly coordinating counterion leads to the change in color from green to red due to the formation of diiron(III)-μ-hydroxo bisporphyrins, 7 (Scheme 9). A number of μ-hydroxo complexes have been synthesized and structurally characterized. Fig. 23 shows the molecular structure of one such complex (**7**·I_3) and its ^{1}H NMR spectrum which clearly shows the signature of both high-spin and intermediate-spin Fe(III) centers. On going from the μ-oxo to the hydroxo complex, there is an increase in the Fe–O bond length while the Fe–O(H)–Fe unit becomes further bent which resulted in the closer approach of the two porphyrin rings. The interaction of two such rings in the μ-hydroxo complex has resulted in unequal core deformation (Fig. 24) with the eventual stabilization of two different spin states of iron in a single

Table 1 Selected geometrical parameters

Complex	Fe–N_p[a]	Fe–O[b]	Fe–O–Fe[c]	Fe···Fe[d]	Δ_{24}^{Fe}[e]	Δ_{24}[f]	Φ[g]	Θ[h]	Closest contact[b]	Ref.
6a·CH_3CN	2.070(3)	1.774(2)	147.9(1)	3.409	0.57	0.20	16.1	25.0	3.016(5)	7*b*,10*b*
6a·$C_6H_5CH_3$	2.076(3)	1.767(2)	151.1(1)	3.423	0.54	0.18	16.4	21.2	3.042(5)	7*b*,10*b*
6b Core-I	2.089(3)	1.785(3)	150.9(2)	3.453	0.61	0.14	0.6	27.7	3.111(8)	7*b*,10*b*
Core-II	2.081(4)	1.781(3)			0.65					
$[Fe^{III}(OEP)]_2O$ (monoclinic)	2.080(5)	1.755(10)	176.2(2)	3.508	0.54	0.03	16.8	2.7	3.680	27
$[Fe^{III}(OEP)]_2O$ (triclinic)	2.077(3)	1.756(3)	172.2(2)	3.503	0.50	0.05	17.0	7.3	3.744	27

[a] Average value in Å. [b] Distance (in Å). [c] Angle (in °). [d] Nonbonding distance (in Å) between two Fe(III) centers in a molecule. [e] Displacement of iron (in Å) from the least-squares plane of the $C_{20}N_4$ porphyrinato core. [f] Average displacement of the 24 atoms (in Å) from the least-squares plane of the $C_{20}N_4$ porphyrinato core. [g] Average of the four N–Fe–Fe′–N′ dihedral angles (in °). [h] Angle (in °) between the two least-squares planes of the $C_{20}N_4$ porphyrinato core.

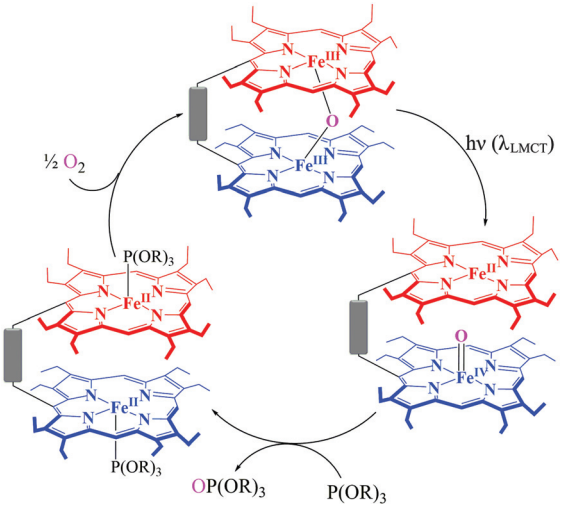

Scheme 8

molecular framework.[11] Also, spin states have been found to be dependent on the counter ions used and are reversibly interconvertable. The μ-hydroxo complexes exhibit weak antiferromagnetic coupling in contrast to the very strong exchange interactions in the corresponding μ-oxo dimer. However, similar μ-hydroxo complexes from the monoporphyrin counterparts have both the iron centers in the same spin state.[29] These differences are believed to be due to stronger inter-heme interactions in the porphyrin dimer. Further studies are in progress.

3. Summary and outlook

There is a high level of conservation of the heme structural arrangement throughout in various multi-heme cytochromes. The functional properties of such an important and widely distributed family are largely determined by the relative arrangement of the heme centers and their inter-macrocycle interactions which decay steeply with the Fe–Fe distance. Understanding the significance of these structural motifs is, however, hindered by the presence of a relatively large number of heme units along with the efficient coupling between them.

This Perspective presents a brief overview of our attempts to unravel the effects of heme–heme interactions using an

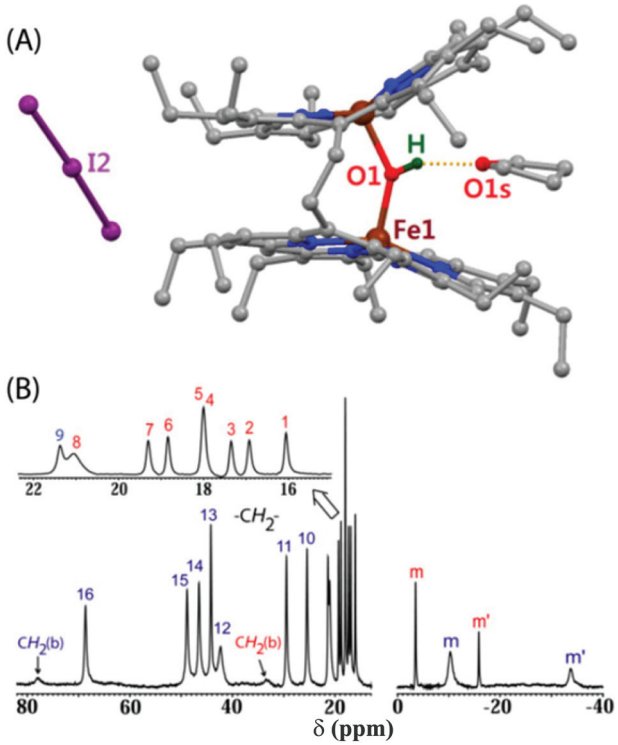

Fig. 23 (A) Molecular structure (at 100 K) of 7·I_3 showing all non-hydrogen atoms (all of the hydrogens except for the μ-hydroxo proton have been omitted for clarity) and (B) its ^{1}H NMR spectrum in $CDCl_3$ at 295 K.

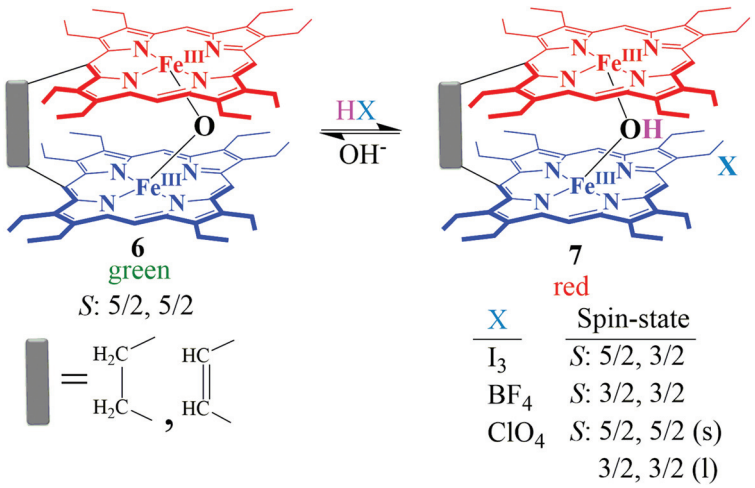

Scheme 9

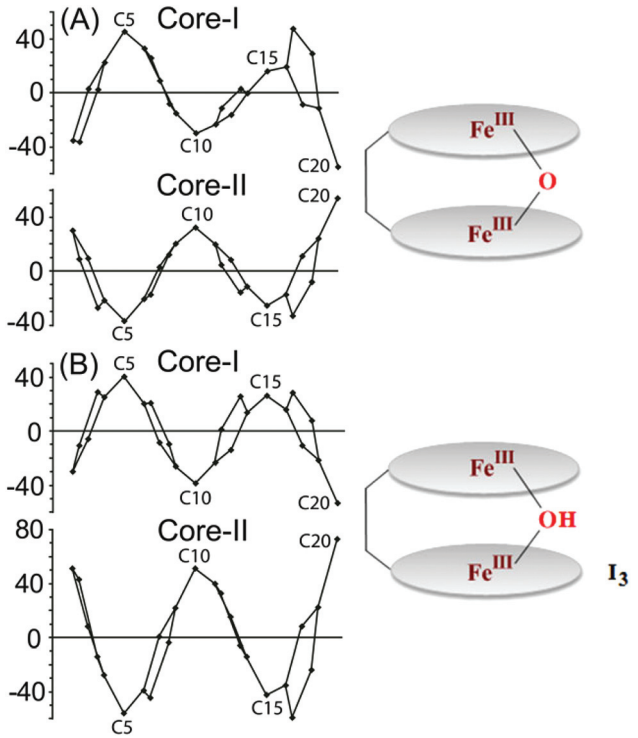

Fig. 24 Out-of-plane displacements (in units of 0.01 Å) of the porphyrin core atoms from the mean porphyrin plane (24 atoms) of (A) **6a**, and (B) **7**·I_3.

ethane-bridged porphyrin dimer as a model of diheme centers. The porphyrin macrocycle in a diheme complex is found to be more distorted, compared to its monoheme analog. Changing the electronic nature of the axial ligand and its substituents has been found to play a crucial role in the nature of shift of the Fe(III)/Fe(II) redox couple while the inter-ring interaction decides the extent of such a shift. Such a variation of the Fe(III)/Fe(II) redox potential, as a result of heme–heme interactions, would be a very useful vehicle for tuning the redox potential of the di/multiheme proteins and their functions. From the results presented it can be concluded that inter-ring interaction is a potent tool to modulate various properties of the heme centers *viz.*, porphyrin ring deformation, axial ligand strength, metal spin state, redox potential, and reactivity as compared to its monoheme counterparts. Thus, it can be said that the presence of more than one heme center provides Nature with a further tool to modulate various properties. However, the exact nature of such inter-heme interactions, which can be attributed to the combinations of a variety of phenomena related to steric, electrostatic, dispersion interactions *etc.*, is still unclear and would require further investigations which are in progress.

The large differences in the structural, chemical, and electrochemical properties of the diheme, as compared to its monoheme analog, provide unequivocal evidence of the role played by heme–heme interactions. We wish to extend the work further from the diheme to triheme and so on in order to understand how the successive addition of the heme centers influences the structure and properties at the individual heme centers. Such a study would be useful in understanding various aspects of Nature's sophisticated design of multiheme centers. Also, the integration of the theoretical approach with experimental work to determine the effects of such interactions would be highly beneficial in elucidating many of the unanswered questions. We thus hope that this Perspective would attract many researchers into this important field of understanding the multiheme proteins.

Acknowledgements

The research contributions of the past and present members (Dr. Sudip Kumar Ghosh, Dr. Ranjan Patra, Dr. Arvind Chaudhary, Dr. Susovan Bhowmik, Dr. Soumyajit Dey, Dipankar Sahoo and Firoz Shah Tuglak Khan) of the group related to the project is greatfully acknowledged. The authors thank the Science and Engineering Research Board (SERB), New Delhi and the Council of Scientific and Industrial Research (CSIR), New Delhi for financial support. D.S. thanks University Grants Commission (UGC), India for his fellowship.

References

1 (*a*) J. Liu, S. Chakraborty, P. Hosseinzadeh, Y. Yu, S. Tian, I. Petrik, A. Bhagi and Y. Lu, *Chem. Rev.*, 2014, **114**, 4366–4469; (*b*) C. M. Paquete and R. O. Louro, *Acc. Chem. Res.*, 2014, **47**, 56–65; (*c*) C. M. Soares and A. M. Baptista, *FEBS Lett.*, 2012, **586**, 510–518; (*d*) B. M. Fonseca, C. M. Paquete, C. A. Salgueiro and R. O. Louro, *FEBS Lett.*, 2012, **586**, 504–509; (*e*) J. A. Mayfield, C. A. Dehner and J. L. DuBois, *Curr. Opin. Chem. Biol.*, 2011, **15**, 260–266; (*f*) C. M. Paquete and R. O. Louro, *Dalton Trans.*, 2010, **39**, 4259–4266; (*g*) H. Akutsu and Y. Takayama, *Acc. Chem. Res.*, 2007, **40**, 171–178; (*h*) L. Shi, T. C. Squier, J. M. Zachara and J. K. Fredrickson, *Mol. Microbiol.*, 2007, **65**, 12–20; (*i*) C. G. Mowat and S. K. Chapman, *Dalton Trans.*, 2005, 3381–3389; (*j*) I. A. Pereira and A. V. Xavier, in *Encyclopedia of Inorganic Chemistry*, ed. R. B. King, John Wiley & Sons, New York, 2005, vol. 5, pp. 3360–3376; (*k*) J. M. Stevens, O. Daltrop, J. W. A. Allen and S. J. Ferguson, *Acc. Chem. Res.*, 2004, **37**, 999–1007.

2 (*a*) M. Breuer, K. M. Rosso and J. Blumberger, *Proc. Natl. Acad. Sci. U. S. A.*, 2014, **111**, 611–616; (*b*) S. Sharma, G. Cavallaro and A. Rosato, *J. Biol. Inorg. Chem.*, 2010, **15**, 559–571; (*c*) M. Pessanha, E. L. Rothery, C. S. Miles, G. A. Reid, S. K. Chapman, R. O. Louro, D. L. Turner, C. A. Salgueiro and A. V. Xavier, *Biochim. Biophys. Acta*, 2009, **1787**, 113–120; (*d*) C. M. Paquete, D. L. Turner, R. O. Louro, A. V. Xavier and T. Catarino, *Biochim. Biophys. Acta*, 2007, **1767**, 1169–1179.

3 (*a*) K. E. Ellis, K. E. Frato and S. J. Elliott, *Biochemistry*, 2012, **51**, 10008–10016; (*b*) G. S. Pulcu, K. E. Frato,

R. Gupta, H.-R. Hsu, G. A. Levine, M. P. Hendrich and S. J. Elliott, *Biochemistry*, 2012, **51**, 974–985; (*c*) M. Hoffmann, J. Seidel and O. Einsle, *J. Mol. Biol.*, 2009, **393**, 951–965; (*d*) A. Echalier, T. Brittain, J. Wright, S. Boycheva, G. B. Mortuza, V. Fülöp and N. J. Watmough, *Biochemistry*, 2008, **47**, 1947–1956; (*e*) G. W. Pettigrew, A. Echalier and S. R. Pauleta, *J. Inorg. Biochem.*, 2006, **100**, 551–567; (*f*) A. Brige, D. Leys, T. E. Meyer, M. A. Cusanovich and J. J. Van Beeumen, *Biochemistry*, 2002, **41**, 4827–4836; (*g*) A. Kadziola and S. Larsen, *Structure*, 1997, **5**, 203–216; (*h*) P. M. Matias, J. Morais, A. V. Coelho, R. Meijers, A. Gonzalez, A. W. Thompson, L. Sieker, J. LeGall and M. A. Carrondo, *J. Biol. Inorg. Chem.*, 1997, **2**, 507–514.

4 (*a*) F. M. Stone and C. B. Coulter, *J. Gen. Physiol.*, 1932, **15**, 629–639; (*b*) L. Smith, *J. Biol. Chem.*, 1959, **234**, 1571–1574; (*c*) P. M. Matias, A. V. Coelho, F. M. Valente, D. Placido, J. LeGall, A. V. Xavier, I. A. Pereira and M. A. Carrondo, *J. Biol. Chem.*, 2002, **277**, 47907–47916.

5 (*a*) O. Einsle, A. Messerschmidt, P. Stach, G. P. Bourenkov, H. D. Bartunik, R. Huber and P. M. H. Kroneck, *Nature*, 1999, **400**, 476–480; (*b*) T. M. Iverson, D. M. Arciero, A. B. Hooper and D. C. Rees, *J. Biol. Inorg. Chem.*, 2001, **6**, 390–397; (*c*) D. Heitmann and O. Einsle, *Biochemistry*, 2005, **44**, 12411–12419; (*d*) H. R. Gibson, C. G. Mowat, C. S. Miles, B.-R. Li, D. Leys, G. A. Reid and S. K. Chapman, *Biochemistry*, 2006, **45**, 6363–6371; (*e*) R. S. Hartshorne, B. N. Jepson, T. A. Clarke, S. J. Field, J. Fredrickson, J. Zachara, L. Shi, J. N. Butt and D. J. Richardson, *J. Biol. Inorg. Chem.*, 2007, **12**, 1083–1094; (*f*) D. Leys, T. E. Meyer, A. S. Tsapin, K. H. Nealson, M. A. Cusanovich and J. J. Van Beeumen, *J. Biol. Chem.*, 2002, **277**, 35703–35711; (*g*) M. V. Pattarkine, J. J. Tanner, C. A. Bottoms, Y.-H. Lee and J. D. Wall, *J. Mol. Biol.*, 2006, **358**, 1314–1327; (*h*) I. Bento, V. H. Teixeira, A. M. Baptista, C. M. Soares, P. M. Matias and M. A. Carrondo, *J. Biol. Chem.*, 2003, **278**, 36455–36469.

6 (*a*) S. Brahma, S. A. Ikbal and S. P. Rath, *Inorg. Chim. Acta*, 2011, **372**, 62–70; (*b*) S. Dey and S. P. Rath, *Dalton Trans.*, 2014, **43**, 2301–2314.

7 (*a*) S. Bhowmik, S. K. Ghosh and S. P. Rath, *Chem. Commun.*, 2011, **47**, 4790–4792; (*b*) S. K. Ghosh, R. Patra and S. P. Rath, *Inorg. Chem.*, 2010, **49**, 3449–3460.

8 (*a*) S. Bhowmik, S. Dey, D. Sahoo and S. P. Rath, *Chem. – Eur. J.*, 2013, **19**, 13732–13744; (*b*) S. Bhowmik, D. Sil, R. Patra and S. P. Rath, *J. Chem. Sci.*, 2011, **123**, 827–837.

9 D. Sil, F. S. T. Khan and S. P. Rath, *Inorg. Chem.*, 2014, **53**, 11925–11936.

10 (*a*) S. K. Ghosh, R. Patra and S. P. Rath, *Inorg. Chim. Acta*, 2010, **363**, 2791–2799; (*b*) S. K. Ghosh, R. Patra and S. P. Rath, *Inorg. Chem.*, 2008, **47**, 10196–10198.

11 (*a*) S. K. Ghosh, S. Bhowmik, D. Sil and S. P. Rath, *Chem. – Eur. J.*, 2013, **19**, 17846–17859; (*b*) S. Bhowmik, S. K. Ghosh, S. Layek, H. C. Verma and S. P. Rath, *Chem. – Eur. J.*, 2012, **18**, 13025–13037; (*c*) S. K. Ghosh and S. P. Rath, *J. Am. Chem. Soc.*, 2010, **132**, 17983–17985; (*d*) M. A. Sainna, D. Sil, D. Sahoo, B. Martin, S. P. Rath, P. Comba and S. P. de Visser, *Inorg. Chem.*, 2015, **54**, 1919–1930.

12 (*a*) S. Brahma, S. A. Ikbal and S. P. Rath, *Inorg. Chem.*, 2014, **53**, 49–62; (*b*) S. Brahma, S. A. Ikbal, A. Dhamija and S. P. Rath, *Inorg. Chem.*, 2014, **53**, 2381–2395; (*c*) S. A. Ikbal, S. Brahma and S. P. Rath, *Chem. Commun.*, 2014, **50**, 14037–14040; (*d*) S. A. Ikbal, S. Brahma and S. P. Rath, *Chem. Commun.*, 2015, **51**, 895–898; (*e*) S. Brahma, S. A. Ikbal, S. Dey and S. P. Rath, *Chem. Commun.*, 2012, **48**, 4070–4072.

13 (*a*) A. Chaudhary and S. P. Rath, *Chem. – Eur. J.*, 2012, **18**, 7404–7417; (*b*) A. Chaudhary and S. P. Rath, *Chem. – Eur. J.*, 2011, **17**, 11478–11487; (*c*) P. Mondal, A. Chaudhary and S. P. Rath, *Dalton Trans.*, 2013, **42**, 12381–12394; (*d*) P. Mondal and S. P. Rath, *Isr. J. Chem.*, 2015, **55**, DOI: 10.1002/ijch.201500014; (*e*) A. Chaudhary, R. Patra and S. P. Rath, *Indian J. Chem.*, 2011, **50A**, 1436–1442; (*f*) A. Chaudhary, S. A. Ikbal, S. Brahma and S. P. Rath, *Polyhedron*, 2013, **52**, 761–769; (*g*) S. A. Ikbal, S. Brahma, A. Dhamija and S. P. Rath, *J. Chem. Sci.*, 2014, **126**, 1451–1461.

14 D. Arnold, A. W. Johnson and M. Winter, *J. Chem. Soc., Perkin Trans. 1*, 1977, 1643–1647.

15 (*a*) J. P. Collman, P. S. Wagenknecht and J. E. Hutchison, *Angew. Chem., Int. Ed. Engl.*, 1994, **33**, 1537–1554; (*b*) J. Rosenthal and D. G. Nocera, *Acc. Chem. Res.*, 2007, **40**, 543–553; (*c*) P. D. Harvey, C. Stern, C. P. Gros and R. Guilard, *Coord. Chem. Rev.*, 2007, **251**, 401–428.

16 (*a*) V. V. Borovkov, J. M. Lintuluoto and Y. Inoue, *Tetrahedron Lett.*, 1999, **40**, 5051–5054; (*b*) V. V. Borovkov, J. M. Lintuluoto and Y. Inoue, *J. Phys. Chem. B*, 1999, **103**, 5151–5156; (*c*) K.-I. Sugiura, G. V. Ponomarev, S. Okubo, A. Tajiri and Y. Sakata, *Bull. Chem. Soc. Jpn.*, 1997, **70**, 1115–1123.

17 M. Kasha, H. R. Rawls and M. A. E. Bayoumi, *Pure Appl. Chem.*, 1965, **11**, 371–392.

18 I. Fujii, V. V. Borovkov and Y. Inoue, *Anal. Sci.*, 2006, **22**, x77–x78.

19 (*a*) G. A. Hembury, V. V. Borovkov, J. M. Lintuluoto and Y. Inoue, *Chem. Lett.*, 2003, **32**, 428–429; (*b*) V. Borokov, J. M. Lintuluoto and Y. Inoue, *Helv. Chim. Acta*, 1999, **82**, 919–934.

20 (*a*) R. Weiss, A. Gold and J. Terner, *Chem. Rev.*, 2006, **106**, 2550–2579; (*b*) M. Nakamura, *Coord. Chem. Rev.*, 2006, **250**, 2271–2294; (*c*) D. Sahoo, M. G. Quesne, S. P. de Visser and S. P. Rath, *Angew. Chem., Int. Ed.*, 2015, **54**, 4796–4800; (*d*) R. Patra, D. Sahoo, S. Dey, D. Sil and S. P. Rath, *Inorg. Chem.*, 2012, **51**, 11294–11305; (*e*) R. Patra, S. Bhowmik, S. K. Ghosh and S. P. Rath, *Dalton Trans.*, 2010, **39**, 5795–5806; (*f*) R. Patra, A. Chaudhary, S. K. Ghosh and S. P. Rath, *Inorg. Chem.*, 2010, **49**, 2057–2067; (*g*) R. Patra and S. P. Rath, *Inorg. Chem. Commun.*, 2009, 515–519; (*h*) R. Patra, A. Chaudhary, S. K. Ghosh and S. P. Rath, *Inorg. Chem.*, 2008, **47**, 8324–8335.

21 (*a*) H. Masuda, T. Taga, K. Osaki, H. Sugimoto, Z. Yoshida and H. Ogoshi, *Inorg. Chem.*, 1980, **19**, 950–955; (*b*) N. Xu, D. R. Powell and G. B. Richter-Addo, *Acta Crystallogr., Sect. E: Struct. Rep. Online*, 2008, **64**, m1366; (*c*) A. D. Boersma and H. M. Goff, *Inorg. Chem.*, 1982, **21**, 581–586.

22 C. A. Reed and F. Guiset, *J. Am. Chem. Soc.*, 1996, **118**, 3281–3282.

23 (*a*) D. Kanamori, Y. Yamada, A. Onoda, T. Okamura, S. Adachi, H. Yamamoto and N. Ueyama, *Inorg. Chim. Acta*, 2005, **358**, 331–338; (*b*) A. M. Helms, W. D. Jones and G. L. McLendon, *J. Coord. Chem.*, 1991, **23**, 351–359; (*c*) N. Ueyama, N. Nishikawa, Y. Yamada, T. Okamura and A. Nakamura, *Inorg. Chim. Acta*, 1998, **283**, 91–97; (*d*) M. P. Byrn, C. J. Curtis, Y. Hsiou, S. I. Khan, P. A. Sawin, S. K. Tendick, A. Terzis and C. E. Strouse, *J. Am. Chem. Soc.*, 1993, **115**, 9480–9497.

24 K. M. Miller and C. E. Strouse, *Acta Crystallogr., Sect. C: Cryst. Struct. Commun.*, 1984, **40**, 1324–1327.

25 (*a*) *Cytochrome P450: Structure, Mechanism, and Biochemistry*, ed. P. R. Ortiz de Montellano, Kluwer Academic/Plenum Publishers, New York, 3rd edn, 2005; (*b*) I. G. Denisov, T. M. Makris, S. G. Sligar and I. Schlichting, *Chem. Rev.*, 2005, **105**, 2253–2277.

26 T. E. Clement, D. J. Nurco and K. M. Smith, *Inorg. Chem.*, 1998, **37**, 1150–1160.

27 B. Cheng, J. D. Hobbs, P. G. Debrunner, J. Erlebacher, J. A. Shelnutt and W. R. Scheidt, *Inorg. Chem.*, 1995, **34**, 102–110.

28 (*a*) J. Rosenthal, T. D. Luckett, J. M. Hodgkiss and D. G. Nocera, *J. Am. Chem. Soc.*, 2006, **128**, 6546–6547; (*b*) J. Rosenthal, J. Bachman, J. L. Dempsey, A. J. Esswein, T. G. Gray, J. M. Hodgkiss, D. R. Manke, T. D. Luckett, B. J. Pistorio, A. S. Veige and D. G. Nocera, *Coord. Chem. Rev.*, 2005, **249**, 1316–1326.

29 (*a*) D. R. Evans and C. A. Reed, *J. Am. Chem. Soc.*, 2000, **122**, 4660–4667; (*b*) D. R. Evans, R. S. Mathur, K. Heerwegh, C. A. Reed and Z. Xie, *Angew. Chem., Int. Ed. Engl.*, 1997, **36**, 1335–1337; (*c*) W. R. Scheidt, B. Cheng, M. K. Safo, F. Cukiernik, J.-C. Marchon and P. G. Duebrunner, *J. Am. Chem. Soc.*, 1992, **114**, 4420–4421.